METEOROLOGICAL APPLICATIONS
Meteorol. Appl. **24**: 260–267 (2017)
Published online in Wiley Online Library
(wileyonlinelibrary.com) DOI: 10.1002/met.1624

RMetS
Royal Meteorological Society

Documentation of atmospheric constants over Niamey, Niger: a theoretical aid for measuring instruments

Moses Eterigho Emetere* and Marvel Lola Akinyemi
Department of Physics, Covenant University, Ota, Nigeria

ABSTRACT: The frequent failures of ground measuring devices, e.g. radiosondes, weather stations, in developing regions is worrisome. From the literature, established projects such as the Aerosol Robotic Network (AERONET) and the African Monsoon Multidisciplinary Analyses (AMMA) are burdened by the same challenge. At the moment, the AERONET and AMMA databases show a large volume of data loss. With only about 47% of data available to scientists, it is evident that accurate nowcasts or forecasts cannot be guaranteed. It is proposed that the challenge is not measuring device design error but systemic, i.e. the configuration of accurate calibration constants in the compact flash card of the devices. The calibration constants of most radiosonde or weather stations are not compatible with the atmospheric conditions of the West African climate. A dispersion model was developed to incorporate salient mathematical representations such as the unified number. The unified number was derived to describe the turbulence of aerosol transport in the frictional layer of the lower atmosphere. A 14 year dataset from the Multi-angle Imaging SpectroRadiometer was tested using the dispersion model. A yearly estimation of the atmospheric constants over Niamey using the model was obtained with about 87.5% accuracy. This further revealed that the average atmospheric constants for Niamey, Niger, are $a_1 = 0.77975$ and $a_2 = 0.693021$ and the tuning constants are $n_1 = 0.140187$ and $n_2 = 0.759236$. Also, the yearly atmospheric constants confirmed that the lower atmosphere of Niamey is very dynamic. Hence, it is recommended that radiosonde and weather station manufacturers should constantly review the atmospheric constants over a geographical location to enable about 80% data retrieval.

KEY WORDS atmospheric constant; dispersion model; unified number; aerosol; Niamey

Received 2 March 2016; Revised 29 July 2016; Accepted 16 August 2016

1. Introduction

The atmosphere is made up of a non-uniform spread of minute gas molecules or suspended particles in the form of liquid, gas or solid (Emetere, 2013; Emetere and Akinyemi, 2013). The spread of the particulates depends on the aerosol ejection sources present in the atmosphere or on the Earth (Emetere *et al.*, 2015a, 2015b). The spread of aerosol over a region scatters or absorbs light from the Sun. Other atmospheric constituents that scatter or absorb light include methane, ozone, nitrous oxides, carbon dioxide and water vapour. The atmospheric constituents present in the atmosphere create several refractive indices for light and signals (Figure 1).

The presence of a multiple refractive index which emerges from turbulent layers in the troposphere (Wilson *et al.*, 2014) affects the functionality of ground measuring devices and satellite sensors *via* signal attenuation. For example, the African Monsoon Multidisciplinary Analyses campaign in Africa (which has been established to improve existing knowledge of the West African monsoon and its variability) adopted various radiosondes for the campaign. Each radiosonde was selected on the basis of the bias to relative humidity measurements. The various radiosonde modifications did not abate the loss of data. The Aerosol Robotic Network campaign in West Africa (which is a federation of ground-based remote sensing aerosol networks) had a similar challenge of malfunctioning sondes. This led to the loss of over 53% of dataset volume in West Africa. Some scientists (Bock *et al.*, 2008) adduced that some of the sondes had design errors. However, in this research, it is proposed that the multiple refractive indices influence atmospheric measurements. Hence, most unsuccessful campaigns may not be directly associated with the measuring instrument but with the inability of the manufacturer to compute accurate calibration constants in the embedded compact flash card. The card contains computational

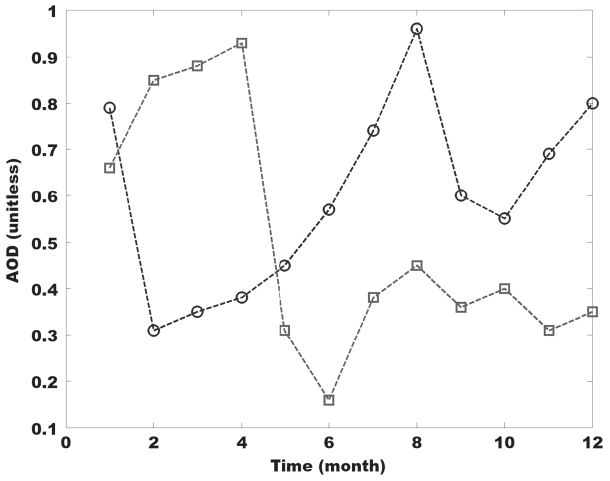

Figure 1. Disparity between ground and satellite measurements. AOD, aerosol optical depth. -⊖-, ground AOD; -⊟-, satellite AOD.

* Correspondence: M. E. Emetere, Department of Physics, Covenant University, Ota, Nigeria. E-mail: emetere@yahoo.com

programming or codes which include the calibration constants. The primary function of the calibration constants is to transform the signals from the sensor into real units. The real units in the form of datasets are retrieved and logged onto a control processing unit or a designated website for further use.

Bock *et al.* (2008) documented the biases of radiosondes except for MODEM M2K2 sondes whose humidity biases are not known. Vaisala RS80-A sondes have been diagnosed to have large dry biases while Vaisala RS92 sondes have been diagnosed to have weakly moist biases. The unknown biases of the MODEM M2K2 sondes and the loss of TEMP messages from reliable ground and satellite observations is further affirmation of the need to document the atmospheric constants over a geographical location such as Niamey, Niger (Nuret *et al.*, 2008). To obtain the atmospheric or calibration constants over a geographical location, long-term satellite or ground observations of aerosol and clouds are essential. Previously, calibration constants were obtained from standard laboratory lamps (Kiedron *et al.*, 1999) with low success, i.e. leading to the loss of TEMP messages.

The West African climate system is unique (Strauss, 2012); hence long-term satellite or ground observations of aerosols are needed to design and develop a mathematical model that will incorporate the independent atmospheric motion vectors (Agustı-Panareda *et al.*, 2010) and the inability of moisture convergence over the Sahel region (Meynadier *et al.*, 2010). Emetere *et al.* (2015b) explained that the collective impacts of moving aerosol layers in the atmosphere were capable of decreasing satellite and ground data retrieval due to the changing refractivity of interactive signals in its optical and microwave sensors. This phenomenon is responsible for the disparity between satellite and ground measurements (Figure 1).

In previous research (Emetere *et al.*, 2015b), a mathematical model was designed that operates on a parametric retrieval mode. In the current study, the model was developed to obtain the atmospheric constants over Niamey. From the literature, the atmospheric constants are dependent on a defined geographical location (see Table 1) and are dynamic with respect to season. Atmospheric constants may appear with different nomenclature, e.g. solar constant, multiplier constant, tuning constant and ageing/growth rate constant. The use of accurate atmospheric constant values in the configuration or calibration of automatic ground station and satellite sensors is challenging because it requires a sound knowledge of the configuration language. For example, some radiosonde codes are written in the Py6S Python interface (Python, 2015).

As discussed earlier, one of the efficient ways to obtain calibration constants is to study long-term satellite or ground observations of aerosols *via* the aerosol model. For example, Schotland and Lea (1986) used dual aerosol models to determine the solar constant. The first model was characterized by a mixed atmospheric boundary layer with corresponding scale height of 1 km while the second model was used to describe a stable atmosphere above 3 km. The results obtained from the two aerosol models showed a small difference in the solar constant bias errors between different tropospheric settings.

A multiplier constant is used in automatic weather stations to monitor the aerosol distribution at certain altitudes (Welton *et al.*, 2002; Python, 2015). Every analogue sensor uses its specific multiplier constant and offset for converting analogue data (Hendrik, 2008). The ageing/growth rate constant is another salient parameter required for configuring ground/satellite station measuring devices. It expresses the distribution and lifetime of aerosols. Within the tropospheric layer, the shape of the size distribution, the number of aerosol particulates and the chemical composition of the average aerosol particles vary as a function of altitude. This makes it a herculean task to estimate the various constants mentioned. Since the occurrences in the Stokes' Region differ, the values of the solar constant, multiplier constant, tuning constant and ageing/growth rate constant differ with respect to geographical region as established in Table 1.

The use of automatic weather stations in developing regions such as Niamey without reconfiguring the constants encrypted in the compact flash card engenders errors in the measurement. By extension, the errors in measurement affect weather forecast and data assimilation. A poor weather forecast translates to a fall in agricultural, forest and grazing production (Cantelaube and Terres, 2005). Hence, the need to generate reliable constants within Niamey is unique. In Section 2 the model designed earlier (Emetere *et al.*, 2015b) is developed to reflect the unified number derivations and kinetic aerosol layer transport. The methodology adopted to obtain the atmospheric constants over Niamey is discussed in Section 3. The results are illustrated in Section 4.

2. Theoretical background of the study

Emetere and Akinyemi (2013) propounded the 3D plume model. The model was initially used to investigate the pollution from a cement factory. The model showed excellent correspondence with pollutant dispersion and depositions around the factory. The governing equation was given as:

$$\begin{aligned}&\frac{\partial C}{\partial t}+V_x\frac{\partial C}{\partial x}-V_z\frac{\partial C}{\partial z}-V_y\frac{\partial C}{\partial y}\\&=\frac{\partial}{\partial z}\left(K_z\frac{\partial C}{\partial z}\right)+\frac{\partial}{\partial y}\left(K_y\frac{\partial C}{\partial y}\right)+\frac{\partial}{\partial z}\left(K_{z2}\frac{\partial C}{\partial z}\right)\\&+\frac{\partial}{\partial y}\left(K_{y2}\frac{\partial C}{\partial y}\right)-P+S\end{aligned}\tag{1}$$

Here, V is the wind velocity ($\mathrm{m\,s^{-1}}$), P is the air upthrust, x is the wind co-ordinate measured in the wind direction from the source, y is the cross-wind co-ordinate direction, z is the vertical co-ordinate measured from the ground, $C(x, y, z)$ is the mean concentration of diffusing pollutants of a diffusing substance at a point (x, y, z) ($\mathrm{kg\,m^{-3}}$), K_y, K_z are the eddy diffusivities in the direction of the y- and z-axes ($\mathrm{m^2\,s^{-1}}$) and S is the source/sink term ($\mathrm{kg\,m^{-3}\,s^{-1}}$). The logarithmic distribution of the wind speed and the exponential function form of the turbulent diffusivity were incorporated into the refined Equation (1). However, the turbulent diffusivity with its corresponding wind speed cannot be determined by directly using the kriging interpolation method (Zhang *et al.*, 2014):

$$V_z\frac{\partial C}{\partial z}=\frac{\partial}{\partial z}\left(K_z\frac{\partial C}{\partial z}\right)+\frac{\partial}{\partial y}\left(K_y\frac{\partial C}{\partial y}\right)+\frac{\partial}{\partial x}\left(K_z\frac{\partial C}{\partial x}\right)\tag{2}$$

$$V_x\frac{\partial C}{\partial x}=\frac{\partial}{\partial y}\left(K_{y2}\frac{\partial C}{\partial y}\right)+\frac{\partial}{\partial z}\left(K_{z2}\frac{\partial C}{\partial z}\right)+\frac{\partial}{\partial x}\left(K_{z2}\frac{\partial C}{\partial x}\right)\tag{3}$$

Equations (2) and (3) represent the turbulent and the mild dispersion equation, respectively. The mild dispersion equation describes the scenario in the free troposphere while the turbulent dispersion equation describes what happens below the planetary boundary layer.

Emetere *et al.* (2015b) expanded on the usefulness of the study by considering a larger space. Here, the Stokes' Region was explored holistically. In the Stokes' Region the Earth represents a sphere and the aerosols or other moving atmospheric gases or suspended particles are fluid. Since Stokes' law influences

Table 1. Atmospheric constants documented over specific geographical stations.

Reference	Instrument	Calibration constant	Location
Hendrik (2008)	KPC 1/6 ME temp	0.1	Germany
Hendrik (2008)	KPC 1/6 ME temp	0.1	Germany
Hendrik (2008)	14 577 wind speed	0.03125	Germany
Hendrik (2008)	CMP3 pyranometer	75.13148	Germany
Volz (1973)	Remsberg, optical	1.491 (433 nm), 1.499 (533 nm)	North Carolina
Volz (1973)	Remsberg, optical	1.287 (433 nm), 1.324 (533 nm)	Sinai Desert Sano
Luers (1997)	Viasala RS90	0.06	Ohio
Halthore *et al.* (1997)	Vaisala RS-80A sondes	$a = 0.616$, $b = 0.593$ (summer) $a = 0.616$, $b = 0.597$ (winter)	Wallops Island, Virginia
Miloshevich *et al.* (2009)	Vaisala RS92	5.199, 4.372	Colorado

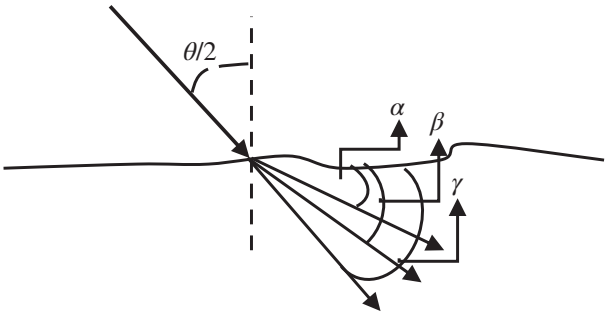

Figure 2. Moving effect of aerosols on refractive indices. α, β and γ are the refracted angles.

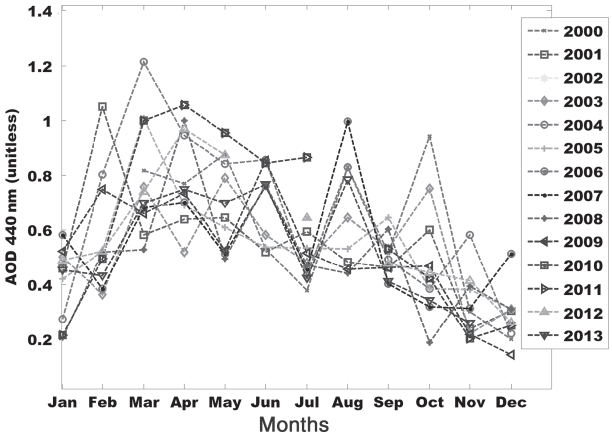

Figure 3. Fourteen years of aerosol optical depth (AOD) patterns at 440 nm.

the Stokes regime, the description of laminar or turbulent flow by the Reynolds or Knudsen number may be somewhat questionable, by their basic definitions. Hence, the need to discuss the unified number is essential in this section. The derivation and validation of the unified number is described in File S1. The effect of the moving aerosol is the solution to Equation (2). The moving aerosol layer creates multiple bending which leads to multiple refractive indices, as illustrated in Figure 2. For example, when a transmitting signal is incident on a moving aerosol layer at an angle $\theta/2$, it has the possibility of bending through one or more refractive angles α, β and γ. This assumption is based on the condition that the aerosol layer thickness is high and heterogeneous in nature, and needs further work (Rotunno, 1993; Sun, 1993).

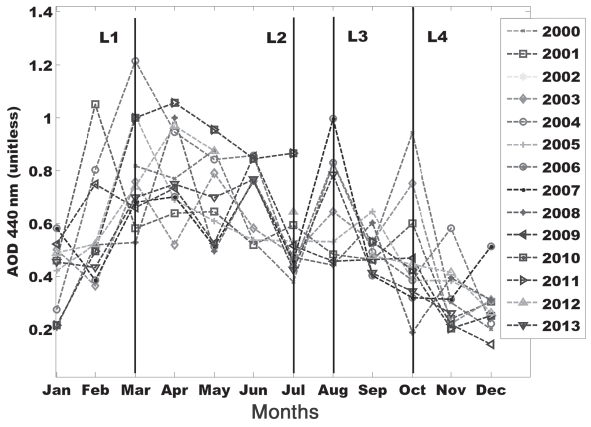

Figure 4. Sectionalized aerosol optical depth (AOD) pattern for 14 years.

Table 2. Reliability of the long-term aerosol dataset.

Year	L1	L2	L3	L4
2000		√	√	√
2001				√
2002	√	√	√	√
2003	√	√	√	√
2004	√	√	√	
2005	√			
2006	√	√	√	
2007	√	√	√	
2008				
2009		√		
2010	√			
2011	√			
2012		√		
2013	√	√	√	

L1, L2, L3 and L4 lines of action are months with the highest frequency within the fourteen years observation.

From the basic refractive index:

$$\sin(\theta/2) = n_1 \cos\alpha$$
$$\sin(\theta/2) = n_2 \cos\beta$$
$$\sin(\theta/2) = n_3 \cos\gamma \quad (4)$$

$$\sin\theta = \{\sin(\theta/2) + \sin(\theta/2)\}\cos(\theta/2) \quad (5)$$

$$\sin(\theta/2) = n_1 \cos\alpha \cos(\theta/2) + n_2 \cos\beta \cos(\theta/2) \quad (6)$$

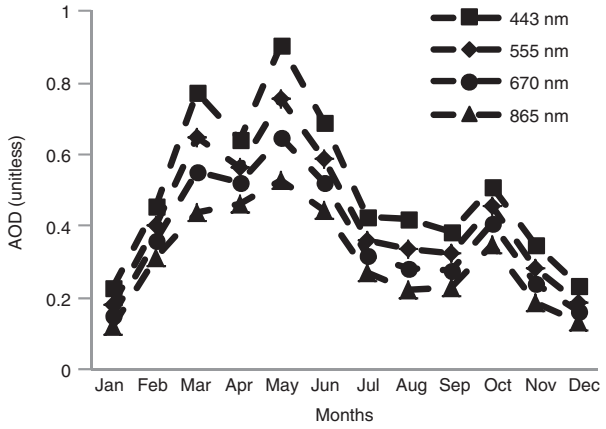

Figure 5. Comparative simulation of Multi-angle Imaging SpectroRadiometer wavelengths.

The relative air mass could be written as $m = 1/\sin\theta$

$$n = C/\sin\theta \tag{7}$$

Hence,

$$C = n^2 \cos\alpha \cos\left(\frac{\theta_i}{2}\right) + n^2 \cos\beta \cos\left(\frac{\theta_1}{2}\right) + \ldots + n^2 \cos\gamma \cos\left(\frac{\theta_n}{2}\right) \tag{8}$$

3. Methodology

The algorithm to obtain the yearly atmospheric constants over Niamey is illustrated in the light of the solution to Equation (2) given by Emetere and Akinyemi (2013) as:

$$C(x,y,z) = a^2 b \cos\left(\frac{n\pi}{2}x + \alpha\right) \cos\left(\frac{n\pi}{2}y + \beta\right) \exp\left(-\frac{V_z}{k_z}z\right) \tag{9}$$

As discussed in Section 1, the methodology adopted in this section is the aerosol dispersion model. The mono-dispersion and poly-dispersion flows were considered by incorporating the Aloyan model into Equations (2) and (3) (Aloyan *et al.*, 2012), i.e. making $N = 2$, $A = \frac{1}{2}\delta_{j3} w_g$, $K_{11} = K_a$, $K_{22} = K_b$, $\psi_1 = \psi_a$, $\psi_2 = \psi_b$, $D_1 = D_a$ and $D_2 = D_b$. This resulted in two mono-dispersion flow equations:

$$\left(\frac{\partial K_a}{\partial z}\frac{\partial \psi_a}{\partial z} + K_a\frac{\partial^2 \psi_a}{\partial z^2} - A\frac{\partial \psi_a}{\partial x}\right) + \frac{\partial \psi_a}{\partial t} = \tau D_a \tag{10}$$

$$\left(\frac{\partial K_b}{\partial z}\frac{\partial \psi_b}{\partial z} + K_b\frac{\partial^2 \psi_b}{\partial z^2} - A\frac{\partial \psi_b}{\partial x}\right) + \frac{\partial \psi_b}{\partial t} = \tau D_b \tag{11}$$

The general term which describes the poly-dispersion flow is given by:

$$\left\{\frac{\partial}{\partial z}\left(K_a + K_b\right)\frac{\partial}{\partial z}\left(\psi_a + \psi_b\right) + K_a\frac{\partial^2 \psi_a}{\partial z^2} + K_b\frac{\partial^2 \psi_b}{\partial z^2} - A\frac{\partial}{\partial x}\left(\psi_a + \psi_b\right)\right\} + \frac{\partial}{\partial t}\left(\psi_a + \psi_b\right) = (Da + Db) \tag{12}$$

Since the dispersion sources are unpredictable on a larger scale, a nearly uniform dispersion from all sources is assumed. The mixed state of both the mono-dispersion and poly-dispersion flows is therefore represented in general terms as:

$$m\frac{\partial K}{\partial z}\frac{\partial \psi}{\partial z} + K\frac{\partial^2 \psi}{\partial z^2} - A\frac{\partial \psi}{\partial x} + \frac{\partial \psi}{\partial t} = \tau D \tag{13}$$

m is the number of dispersion sources. For simplification of the above equation, $\eta = \partial K/\partial z$ and $B = -A\frac{\partial \psi}{\partial x} + \frac{\partial \psi}{\partial t} - \tau D$ Hence, when Equation (13) is wavelength dependent, it becomes:

$$m\eta\frac{\partial \psi(\lambda,t)}{\partial z} + K\frac{\partial^2 \psi(\lambda,t)}{\partial z^2} + B = 0 \tag{14}$$

Let the initial conditions be $\psi(0) = \alpha$, $\psi'(0) = \beta$. The Laplace transform was applied to solve Equation (31):

$$\psi(\lambda,t) = (m\alpha\lambda - \mathrm{B})\cos(m\eta t) + \beta\sin(m\eta t) \tag{15}$$

If the term B is a minimum, i.e. $B = 0$, then:

$$A\frac{\partial \psi(\lambda,t)}{\partial x} + \frac{\partial \psi(\lambda,t)}{\partial t} - \tau D = 0 \tag{16}$$

Applying the Hermite polynomial:

$$\psi(\lambda,t) = \exp\left(2t\lambda - t^2\right) = \exp\left(\lambda^2\right)$$

$$\exp\left\{(\lambda - t)^2\right\} = \sum_{n=0}^{\infty} H_n(\lambda)\frac{t^n}{n}$$

Let $\lambda - t = u$. Then, $t = \lambda - u = 0$ and $-\partial/\partial t = \partial/\partial u$. $-\partial/\partial t = \partial/\partial u$ is substituted into Equation (16) to yield two governing equations:

$$\frac{\partial \psi(\lambda)}{\partial x} = \tau(\lambda) D \tag{17}$$

$$\frac{(1/2)\delta_{j3} w_g}{D} - \frac{1}{D} = \tau(\lambda) \tag{18}$$

To solve for turbulence or laminar flow, the initial and boundary conditions for gravitational settling are:

$$w_g = \begin{cases} U < 0 & v = 0.3 \\ 0 \le U \le 1 & v = 0.7 \\ 1 \le U \le 2 & v = 1.36 \\ 2 \le U \le 5 & v = 2.73 \\ 5 \le U \le 10 & v = 7.57 \\ 10 \le U \le 100 & v = 14.8 \\ U > 100 & v = 30.3 \end{cases} \tag{19}$$

Here, v is the settling velocity ($\mathrm{cm\,s^{-1}}$) and $\delta_{j3} = 1$. Hence, the formulation for the aerosol size distribution from Equation (19) is:

$$\psi(\lambda) = \tau(\lambda) Dx \tag{20}$$

This can be compared with Equation (9):

$$a^2 b \cos\left(\frac{n\pi}{2}x\right)\cos\left(\frac{n\pi}{2}y\right)\exp\left(-\frac{V_z}{k_z}z\right) = \psi(\lambda) = \tau(\lambda) Dx \tag{21}$$

From Equation (21) Dx can be equated to the term on the left hand side:

$$\psi(\lambda) = a^2\tau(\lambda)\cos\left(\frac{n\pi}{2}x\right)\cos\left(\frac{n\pi}{2}y\right) \tag{22}$$

or

$$\psi(\lambda) = ab\tau(\lambda)\cos\left(\frac{n\pi}{2}y\right)\exp\left(-\frac{V_z}{k_z}z\right) \tag{23}$$

or

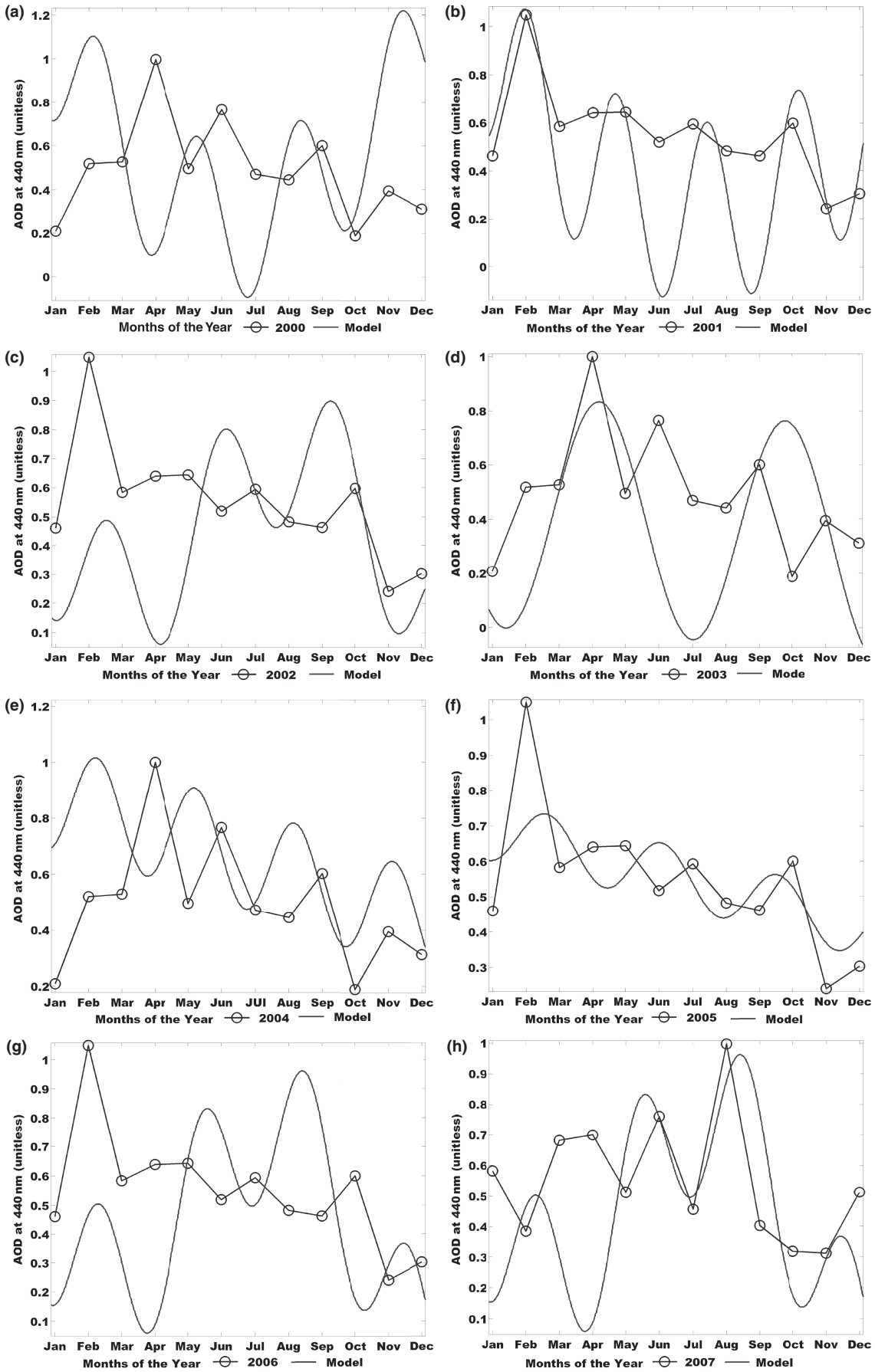

Figure 6. (a)–(n) Atmospheric constant retrieval *via* customized curve fitting.

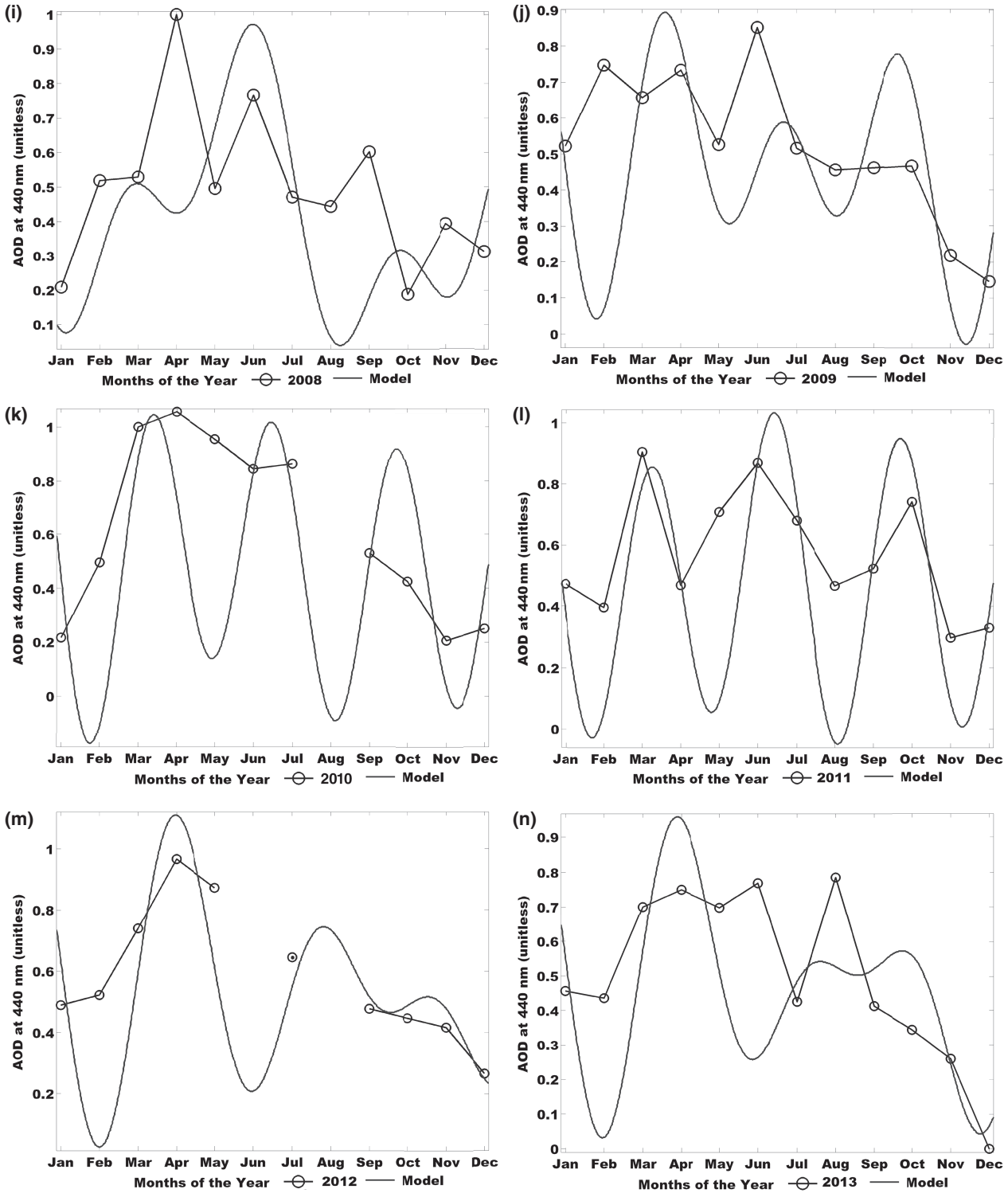

Figure 6. Continued.

$$\psi(\lambda) = ab\tau(\lambda)\cos\left(\frac{n\pi}{2}x\right)\exp\left(-\frac{V_z}{k_z}z\right) \tag{24}$$

Equation (24) is the most valid for the study because of the variability of V_z. Also, when aerosols are deposited into the atmosphere, V_z does not have a significant effect on its lifespan. The mathematical hypothesis used to modify Equations (22)–(24) is provided in File S1.

Hence, the term $\tau(\lambda)$ can be introduced into the cosine *via* the 'abridged trigonometry hypothesis' (Emetere, 2016) shown above:

$$\psi(\lambda) = a^2\cos\left\{\frac{n\pi\tau(\lambda)}{2}x\right\}\cos\left\{\frac{n\pi\tau(\lambda)}{2}y\right\} \tag{25}$$

Applying the principles of multiple refraction expressed in Equation (14), Equation (25) can also be written as:

Table 3. Atmospheric constants for Niamey with errors of ±0.01.

Year	a_1	a_2	n_1	n_2
2000	0.8394 ± 0.01	1.357 ± 0.01	0.1129 ± 0.01	0.8819 ± 0.01
2001	0.8667 ± 0.01	1.137 ± 0.01	0.1074 ± 0.01	0.9848 ± 0.01
2002	0.7035 ± 0.01	0.7578 ± 0.01	0.2388 ± 0.01	0.7797 ± 0.01
2003	0.9213 ± 0.01	0	0	0.4746 ± 0.01
2004	0.6092 ± 0.01	1.192 ± 0.01	0.01576 ± 0.01	0.8934 ± 0.01
2005	0.4084 ± 0.01	1.114 ± 0.01	0.01346 ± 0.01	0.7647 ± 0.01
2006	0.7145 ± 0.01	0.7876 ± 0.01	0.2596 ± 0.01	0.8587 ± 0.01
2007	0.7145 ± 0.01	0.7876 ± 0.01	0.2596 ± 0.01	0.8587 ± 0.01
2008	0.6525 ± 0.01	0.7952 ± 0.01	0.3604 ± 0.01	0.7569 ± 0.01
2009	0.7285 ± 0.01	0.7241 ± 0.01	0.2753 ± 0.01	0.4289 ± 0.01
2010	0.5455 ± 0.01	1.066 ± 0.01	0.1228 ± 0.01	0.6385 ± 0.01
2011	0.3662 ± 0.01	0.9838 ± 0.01	0.6927 ± 0.01	0.6198 ± 0.01
2012	0.7876 ± 0.01	0.7947 ± 0.01	0.4255 ± 0.01	0.5676 ± 0.01
2013	0.7839 ± 0.01	0.7144 ± 0.01	0.4755 ± 0.01	0.5489 ± 0.01

$$\psi(\lambda) = a_1^2 \cos\left\{\frac{n\pi\tau(\lambda)}{2}x\right\}\cos\left\{\frac{n\pi\tau(\lambda)}{2}y\right\} + \ldots + a_n^2 \cos\left\{\frac{n\pi\tau(\lambda)}{2}x\right\}\cos\left\{\frac{n\pi\tau(\lambda)}{2}y\right\} \quad (26)$$

The desired equation, i.e. Equation (26), was inserted into the MATLAB curve fitting tool to obtain the yearly atmospheric constants from the Multi-angle Imaging SpectroRadiometer (MISR) dataset. This technique had been previously adopted for environmental modelling to determine co-efficients or constants from a set of available data (Holzbecher, 2012). The MATLAB curve fitting tool resolves the constants highlighted in Equation (26) numerically and gives a statistical analysis of the MISR dataset. MISR was launched in 1999 to measure the intensity of solar radiation reflected by the planetary surface and atmosphere. The MISR operates in various directions, i.e. at nine different angles (70.5°, 60°, 45.6°, 26.1°, 0°, 26.1°, 45.6°, 60°, 20.5°), and gathers data in four different spectral bands (blue, green, red and near-infrared) of the solar spectrum. The blue band is at wavelength 443 nm, the green band at wavelength 555 nm, the red band at wavelength 670 nm and the infrared band at wavelength 865 nm. MISR acquires images at two different levels of spatial resolution, i.e. the local and global mode. It gathers data at 275 m pixel size in the local mode and at 1.1 km in the global mode. Typically, the blue band is to analyse coastal and aerosol studies. The green band is to analyse bathymetric mapping and estimate peak vegetation. The red band analyses the variable vegetation slopes and the infrared band analyses biomass content and shorelines.

4. Results and discussion

The aerosol optical depth (AOD) for Niamey, Niger, is shown in Figure 3; the AOD pattern follows four major lines L1, L2, L3 and L4 in March, July, August and October respectively. These lines are referred to as 'lines of action', as shown in Figure 4. The lines of action are months with the highest frequency within the 14 years of observation. March, August and October have the peaks of the year while July has the major low. The table of compliance to the lines of action is illustrated in Table 2. Table 2 illustrates the reliability of the long-term aerosol dataset to be used for calibration purposes. Hence, the probability of obtaining reliable results from satellite observations at Niamey, Niger, is 0.518. For this analysis, all the wavelengths, i.e. 440, 555, 670 and 865 nm, available on the MISR dataset were plotted to see the trends or patterns expected for each. However, they all showed the same trend and pattern (Figure 5) but at different values. Hence, the wavelength with the highest AOD was chosen, i.e. 440 nm.

The marked boxes in Table 2 show that 2000, 2002, 2003, 2004, 2006, 2007 and 2013 have a high probability of determining the atmospheric constant. The AOD patterns for 2005, 2008, 2010 and 2011 showed a stable non-conformity. Only 2009 and 2012 showed a distinct non-conformity. Hence, the estimation of the atmospheric constants over Niamey using Equation (26) has the possibility of 87.5% success.

It was clarified in Section 3 that Equation (26) would be fitted into the MATLAB curve fitting tool to resolve the constants for each MISR dataset. The constants obtained *via* the curve fitting tool are referred to as the atmospheric constants, which are shown in Figure 6. In the year 2000 (Figure 6(a)), the proposed model fairly described the MISR data, represented by a solid-unbroken line. The proposed model determined the AOD for 5 months, i.e. March, May, August, September and October. It determined the AOD value for 9 months in 2001 (Figure 6(b)), 5 months in 2002 and 2006 (Figures 6(c) and (g)), 6 months in 2003 to 2005 (Figures 6(d)–(f)), 8 months in 2007 (Figure 6(h)), 7 months in 2008 and 2010 (Figures 6(i) and (k)), 6 months in 2009 and 2011 (Figures 6(j) and (l)), 5 months in 2012 (Figure 6(m)) and 7 months in 2013 (Figure 6(n)). The variation between the satellite and theoretical measurements for each month between 2000 and 2013 is between 2 and 5 months. This shows the effect of undulating weather conditions over the region. The dynamism of the model to comprehend the weather forces of the West Africa meteorology (Emetere *et al.*, 2015a, 2015b, 2015c) is commendable. Thus it can be adopted in generating reliable atmospheric constants.

The atmospheric constants obtained from Figure 6 are given in Table 3.

On average, the atmospheric constants for Niamey, Niger, for 14 years are $a_1 = 0.77975$, $a_2 = 0.693021$, $n_1 = 0.140187$ and $n_2 = 0.759236$. n_1 and n_2 refer to the tuning constants while a_1 and a_2 refer to the atmospheric constants required for the accurate calibration of measuring devices in Niamey, Niger. The constants are configured into the compact flash card which may be written in Python. Therefore, if any of the instruments listed in Table 1 were used for field campaigns, only Vaisala RS-80A sondes may

operate relatively well with many missing or lost data. This is further proof that the failures of sondes over West Africa are a systemic error and not a design error.

5. Conclusion

The designed model (Emetere *et al.*, 2015a) was successfully developed by incorporating salient mathematical conditions which perfectly describe the Stokes regime. The reliability of the 14 year Multi-angle Imaging SpectroRadiometer dataset was tested *via* the aid of 'action lines' which describe months of highest frequency within the dataset. The reliability test affirmed the possibility of 87.5% success when the long-term aerosol dataset is used. The instrumentality of Equation (26) was used to obtain the atmospheric constants *via* the MATLAB curve fitting tool. The curve fitting tool showed that the proposed model could predict a minimum of 5 months and a maximum of 8 months within any year in Niamey. These results further support the authenticity of the atmospheric constants over the troposphere of Niamey. The highest atmospheric and tuning constants were obtained in 2000 and 2013 respectively. These revealed that the average atmospheric constants for Niamey, Niger, are $a_1 = 0.77975$, $a_2 = 0.693021$, $n_1 = 0.140187$ and $n_2 = 0.759236$. Hence, the objective of the work, i.e. to document the atmospheric constants over Niamey, was successfully achieved. This simply means that radiosondes and other measuring instruments can achieve over 80% data acquisition on a daily basis if the atmospheric constants are calibrated accordingly.

Acknowledgements

The authors thank NASA for generously allowing use of their datasets. The authors recognize the partial sponsorship of their host institution. They appreciate the contribution of the reviewers.

Supporting information

The following material is available as part of the online article:

File S1. Appendix.

References

Agustı-Panareda A, Beljaars A, Cardinali C, Genkova I, Thorncroft C. 2010. Impact of assimilating AMMA soundings on ECMWF analyses and forecasts. *Weather Forecasting* **25**: 1142–1160.

Aloyan AE, Arutyunyan VO, Yermakov AN, Zagaynov VA, Mensink C, De Ridder K, et al. 2012. Modeling the regional dynamics of gaseous admixtures and aerosols in the areas of lake Baikal (Russia) and Antwerp (Belgium). *Aerosol Air Qual. Res.* **12**: 707–721.

Bock O, Bouin M-N, Doerflinger E, Collard P, Masson F, Meynadier R, et al. 2008. The West African monsoon observed with ground based GPS receivers during AMMA. *J. Geophys. Res.* **113**: D21105.

Cantelaube P, Terres J-M. 2005. Seasonal weather forecasts for crop yield modelling in Europe. *Tellus A* **57**: 476–487.

Emetere ME. 2013. Modeling of particulate radionuclide dispersion and deposition from a cement factory. *Ann. Environ. Sci.* **7**(6): 71–77.

Emetere ME. 2016. Numerical Modeling of the West Africa Regional Scale Dispersion, Doctoral thesis, Covenant University.

Emetere ME, Akinyemi ML. 2013. Modeling of generic air pollution dispersion analysis from cement factory. *Anal. Univ. Oradea–Ser. Geogr.* **231123-628**: 181–189.

Emetere ME, Akinyemi ML, Akin-Ojo O. 2015a. Aerosol optical depth trends over different regions of Nigeria: thirteen years analysis. *Mod. Appl. Sci.* **9**(9): p267–p279.

Emetere ME, Akinyemi ML, Akinojo O. 2015b. Parametric retrieval model for estimating aerosol size distribution *via* the AERONET, Lagos station. *Environ. Pollut.* **207**(C): 381–390.

Emetere ME, Boyo AO, Akinyemi ML. 2015c. Statistical analysis of the thermal comfort in the urban climate of Ilorin-Nigeria: a three decade event. *Res. J. Fish. Hydrobiol.* **10**(11): 178–185.

Halthore RN, Eck TF, Holben BN, Markham BL. 1997. Sun photometric measurements of atmospheric water vapor column abundance in the 940-nm band. *J. Geophys. Res.* **102**(D4): 4343–4352.

Hendrik Z. 2008. Test and installation of an automatic weather station to provide ground-based FTIR measurements for TCCON, Diploma thesis, Department of SciTec, Precision, Optics, Materials, Environment, University of Applied Science, Jena, Germany.

Holzbecher E. 2012. *Environmental Modeling: Using MATLAB*. Springer: Heidelberg, DOI: 10.1007/978-3-642-22042-5.

Kiedron PW, Michalsky JJ, Berndt JL, Harrison LC. 1999. Comparison of spectra irradiance standards used to calibrate shortwave radiometers and spectroradiometers. *Appl. Opt.* **38**: 2432–2439.

Luers JK. 1997. Temperature error of the Vaisala RS90 radiosonde. *J. Atmos. Oceanic Tech.* **14**: 1520–1532.

Meynadier R, Bock O, Gevois S, Guichard F, Redelsperger JL, Agust´ı-Panareda A, et al. 2010. West African Monsoon water cycle. 2. Assessment of numerical weather prediction water budgets. *J. Geophys. Res.* **115**: D19107.

Miloshevich LM, Vömel H, Whiteman DN, Leblanc T. 2009. Accuracy assessment and correction of Vaisala RS92 radiosonde water vapor measurements. *J. Geophys. Res.* **114**: D11305, doi: 10.1029/2008JD011565.

Nuret M, Lafore JP, Bock O, Guichard F, Agust´ı-Panareda A, Ngamini JB, et al. 2008. Correction of humidity bias for Vaısala RS80 sondes during AMMA 2006 observing period. *J. Atmos. Oceanic Tech.* **25**: 2152–2158.

Python. 2015. http://py6s.readthedocs.org/en/latest/params.html (accessed 6 September 2015).

Rotunno R. 1993. On the linear theory of land and sea breeze. *J. Atmos. Sci.* **40**: 1999–2009.

Schotland RM, Lea TK. 1986. Bias in a solar constant determination by the Langley method due to structured atmospheric aerosol. *Appl. Opt.* **25**: 2486–2492.

Sun WY. 1993. Numerical experiments for advection equation. *J. Comput. Phys.* **108**: 264–271.

Strauss RS. 2012. Vulnerability to climate change in West Africa: adaptive capacity in the regional context. http://reliefweb.int/report/nigeria/vulnerability-climate-change-west-africa-adaptive-capacity-regional-context (accessed 8 June 2014).

Volz FE. 1973. Infrared optical constants of ammonium sulfate, Sahara dust, volcanic pumice, and flyash. *Appl. Opt.* **12**: 564–568.

Wilson R, Luce H, Hashiguchi H, Nishi N, Yabuki Y. 2014. Energetics of persistent turbulent layers underneath mid-level clouds estimated from concurrent radar and radiosonde data. *J. Atmos. Sol. Terr. Phys.* **118**(A): 78–89.

Welton EJ, Kenneth JV, Patricia KQ, Piotr JF, Krzyszt M, James EJ. 2002. Measurements of aerosol vertical profiles and optical properties during INDOEX 1999 using micropulse lidars. *J. Geophys. Res.* **107**(D1): 8019.

Zhang T, Xu N, Guo L, Huang Y, Yong B. 2014. A global atmospheric contaminant transport model based on 3D advection-diffusion equation. *J. Clean Energy Technol.* **2**(1): 43–47.

